



Fatigue behaviour of automatically HFMI-treated welds

Lea Wendler¹ · Daniel Löschner¹ · Imke Engelhardt¹

Received: 31 August 2023 / Accepted: 25 January 2024
© The Author(s) 2024

Abstract

Due to notches, welds are most critical regarding fatigue failure within cyclic loaded constructions. Therefore, various post-weld-treatment techniques like post-weld treatment by high-frequency mechanical impact (HFMI) treatment have been invented to improve the fatigue strength of welded details. The benefit, resulting from HFMI treatment, has already been proven by numerous studies. Since a manual HFMI treatment must be performed by a skilled and trained person to ensure an acceptable treatment quality, an automated application of HFMI treatment is supposed to result in a more reliable and consistent treatment result, which does not depend on the operator. Furthermore, a robotic application of HFMI treatment enables an economic implementation of HFMI treatment of automated welded constructions like offshore wind energy converters and various mechanical components, as these parts do not have to be taken out of the production chain to manually perform HFMI treatment. This paper focuses on the experimental investigation of the fatigue behaviour of automated HFMI-treated welds, using a developed robotic application of the HiFIT device (specific HFMI tool).

Keywords High-frequency mechanical impact (HFMI) · Automation · Weld geometry · Early crack detection · Infrared thermography

Nomenclature

AW	As-welded	$\Delta\vartheta_{\text{nonlin}}$	Difference amount of the nonlinear temperature amplitude
b	Width of the groove of the HFMI-treated weld toe	P	Survival probability
d	Indentation depth of the groove of the HFMI-treated weld toe	r	Radius of the groove of the HFMI-treated weld toe
FAT	Fatigue class	R	Stress ratio
ϑ_{lin}	Linear temperature amplitude	S/N	Nominal stress range S versus cycles to failure N
$\vartheta_{\text{nonlin}}$	Nonlinear temperature amplitude	HFMI	High-frequency mechanical impact treatment
$\Delta\sigma$	Nominal stress range	HFMI-man	Manually performed high-frequency mechanical impact treatment
$\Delta\sigma_{50\%}$	Mean fatigue resistance	HFMI-robo	Automated performed high-frequency mechanical impact treatment
$\Delta\sigma_c$	Reference value of the fatigue strength	N	Number of load cycles
$\Delta\vartheta$	Difference amount of the temperature amplitude	N_f	Number of load cycles to failure
$\Delta\vartheta_{\text{lin}}$	Difference amount of the linear temperature amplitude	N_i	Number of load cycles to technical crack initiation
		N/N_f	Number of load cycles at a specific moment of the fatigue test N versus number of load cycles to failure N_f
		N_i/N_f	Number of load cycles to technical crack initiation N_i versus number of load cycles to failure N_f
		IIW	International Institute of Welding

✉ Lea Wendler
wendler@hm.edu

Daniel Löschner
daniel.loeschner@hm.edu

Imke Engelhardt
imke.engelhardt@hm.edu

¹ Institute for Material and Building Research, University of Applied Science Munich, Munich, Germany

1 Introduction

Various post-weld treatment techniques, like post-weld treatment by high-frequency mechanical impact treatment (HFMI), have been invented to improve the fatigue strength of welds which have, due to the notch effect, a lower fatigue life than the base material. By applying HFMI treatment, the weld toe is plastically deformed by a metal pin, as shown in Fig. 1. Thereby, residual compressive stresses arise within the area of the weld toe, the material is work hardened and the geometrical notch of the weld toe is smoothed. The increase of the fatigue strength, resulting from these effects, has already been proven by numerous studies, like [1–7]. By increasing the fatigue strength of a welded construction, the fatigue life can be extended or otherwise, the plate thickness within an HFMI-treated detail can be reduced by consistent fatigue life. Thus, HFMI treatment contributes to realising resource-efficient constructions.

So far, the application of HFMI treatment in practice has been performed manually. Since the manufacturing process of several welded components like offshore wind-energy converters and various mechanical parts has already been robotised, an automated application of HFMI treatment is necessary to realise an economic HFMI treatment within series production. To ensure an acceptable treatment quality within manual HFMI treatment, the post-weld treatment must be performed by a skilled and trained person. Therefore, an automated application of HFMI treatment is expected to result in a more reliable and consistent treatment quality. Additionally, an automated quality control can be embedded within a robotic HFMI treatment, which also enables a more precise measurement of geometrical quality criteria, compared to a manually performed measurement of the HFMI groove.

Studies on automation of post-weld treatment by high-frequency mechanical impact treatment are yet rare. First

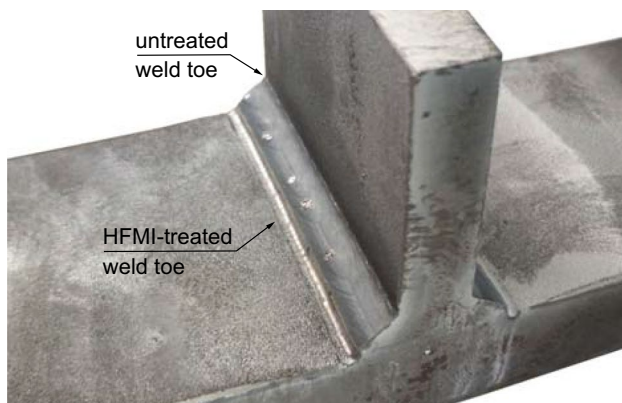


Fig. 1 HFMI-treated weld toe

investigations of the University of Aalborg regarding a robotic HFMI treatment in [8] suggest that an automated application of HFMI treatment, which adapts to irregularities within the course of the weld toe, makes it possible to realise a more consistent treatment quality. Since these results have not been verified by fatigue tests, this paper here focuses on the investigation of the fatigue behaviour of automatically HFMI-treated welds.

2 Automation of post-weld treatment by high-frequency mechanical impact treatment

2.1 State of research

Previous studies on automating the HFMI treatment in [8–10] focused on quality assurance aspects regarding the groove geometry. In [9] and [10], an automated performed HFMI treatment, executed by a robot arm following a straight line, was compared to a manual reference. As the measured groove radii in [10] show, the groove radii generated by automated treatment are significantly more scattered compared to the HFMI groove of the manually treated samples. Regarding the indentation depth, similar results could be found in [9], where the measurement of the automatically treated samples also shows a significantly higher variance. In both cases, the inability of the robotic arm to follow the exact course of the weld toe in contrast to a manual application of the treatment was mentioned as the reason for the larger variance of the robotically generated groove geometry.

As it is necessary for an optimised post-weld treatment result to precisely follow the actual course of the weld toe, in [8], a robotic application of HFMI treatment was developed, which enables to adapt to the irregularities within the course of the weld toe, based on laser scanning the surface. The evaluation of the measured geometry parameters in [8] shows, with the exception of the measured indentation depth, a lower variance for the adaptive robotic-treated weld toes compared to a manually performed treatment. The results in [8] therefore indicate that an adaptive robotic treatment enables a more consistent treatment geometry than a manual HFMI treatment.

2.2 Developed robot adaption of the HiFIT device

To exactly follow the course of the weld toe, the aim was to develop an adaptive robotic treatment tool, which adapts to irregularities within the course of the weld toe. The automated HFMI treatment within this research was performed by a developed robot adaption of the HiFIT device, which is described in [11]. The robot adaption consists of the HiFIT hammer and two laser sensors. One laser sensor is running

ahead and measures the local weld geometry to localise the exact position of the weld toe. Thereby, the HFMI tool is adjusted by the developed software to accurately adapt to the weld toe. The second laser sensor follows the treatment tool and enables a just-in-time quality control by measuring the HFMI groove. As the two laser sensors and the HiFIT tool are installed in one adaption, it is possible to perform a robotic HFMI treatment, as well as an automated quality control in just one run.

3 Test program

In order to evaluate the increase of the fatigue strength, achieved by a robotic HFMI treatment, fatigue tests of automated and manually treated specimens, as well as an as-welded (AW) reference series, were carried out. Table 1 summarises the test program. Concerning the post-weld-treatment, there was a distinction made between the two weld conditions “HFMI-robo” (automated performed HFMI treatment) and “HFMI man” (manually performed HFMI treatment). The two series with manually treated samples vary in the diameter of the pin used for the treatment. Regarding the automated performed treatment, it was meant to try out the robotic application within the robot test application and, if necessary, optimise the treatment parameters afterwards. As the test application of the automated HFMI treatment already showed good results, no further adjustment of the treatment parameters has been made.

3.1 Samples

The notch detail with which the investigations have been carried out is the one-sided transverse stiffener. The specimen geometry is shown in Fig. 2. The samples were fabricated of S355MC (material number 1.0976 according to [12]) by metal active gas welding (MAG). The welding procedure specification is given in Table 2. Additionally, the treatment parameters of the manual and automated treatment

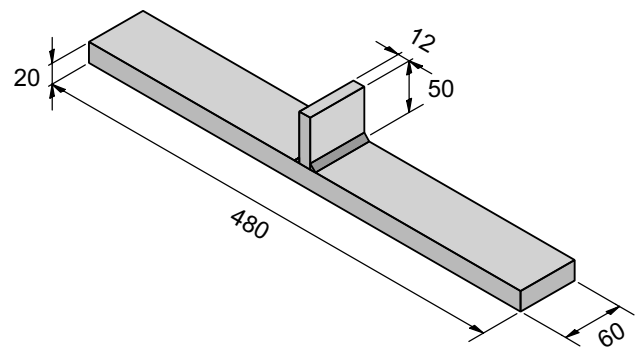


Fig. 2 Dimensions of the specimen

are summarised in Table 3, where the intensity refers to the chosen intensity level setting of the HiFIT device.

As evident from Table 3, different parameters were applied for the manual and automated HFMI treatment. In opposite to an automated HFMI treatment, the operator of a manual treatment can directly react to irregularities within the weld toe by adjusting the contact pressure and the movement of the HiFIT device. In an automated application of the HFMI treatment, that must be realised by the robot adaption. As described in Section 2.2, irregularities within the course of the weld toe are detected using an integrated laser sensor. To ensure a consistent treatment intensity, the robot adaption developed within this research project generates a constant contact pressure [11]. The intensity of an HFMI treatment also depends on the position of the device, the travel speed and the chosen intensity level. Regarding the applied treatment parameters, it should be noted that slower processing at the same intensity level leads to more pin impacts in relation to the same weld length. As the travel speed of the manually performed treatment is significantly lower compared to the automated application, the lower intensity level, chosen for the HFMI-man treatment, matches the higher intensity level of the HFMI-robo treatment. The chosen treatment parameters as well as the result of the automated HFMI treatment were initially tested within a robot test application (see Table 1).

The influence of varying treatment parameters on the improved fatigue strength, achieved by the HFMI treatment, was investigated in previous studies [3, 15, 16]. In all these studies mentioned, the impact of the treatment intensity on the fatigue behaviour was observed to be negligible as long as the treatment parameters were within the appropriate range. Since the treatment parameters used in this study also were within the proper range in both cases according to the manufacturer, the different treatment parameters of the two treatment conditions HFMI-man and HFMI-robo are not supposed to result in significant differences in the fatigue strength.

Table 1 Test program

Series no	Weld condition	Pin diameter (mm)	Number of specimens
No. 1	HFMI-robo (test application)	3	15
No. 2	HFMI-robo (practice application)	3	14
No. 3	HFMI man	4	15
No. 4	HFMI man	3	15
No. 5	AW (reference series)	-	14

Table 2 Welding parameters according to [13] and [14]

Process	Filler metal	Diameter (mm)	Wire feed (m/min)	Current (A)	Voltage (V)	Polarity (-)	Travel speed (cm/min)	Heat input (KJ/cm)	Shielding gas
135	G505MG4Si1	1.2	10.0	300	28.0	DC+	40–50	10–13	M21

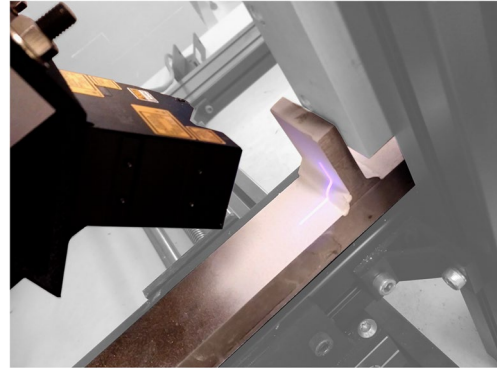
Table 3 HFMI treatment parameters

Weld condition	Pressure (bar)	Speed (mm/min)	Intensity (-)
HFMI-man	7.0	420 (mean value)	1
HFMI-robo	5.5	800	2

**Fig. 3** Specimen installed in testing machine

3.2 Experimental investigations

In order to verify the fatigue strength achieved by an automated application of HFMI treatment compared to a manual treatment, fatigue tests were carried out. The specimens were tested with a constant amplitude loading and a stress ratio of $R=0.1$. As it is explained below, during some of the fatigue tests, infrared sequences were recorded to investigate the crack initiation behaviour. For the evaluation of the infrared data, it is necessary that the loading frequency is coordinated with the recording frequency of the infrared camera. Thus, the fatigue tests with simultaneous thermography measurements were carried out with a test frequency of 7 Hz using a testing machine, shown in Fig. 3, with a maximum load of $F_{\max} = 1000$ kN. The other fatigue tests were performed with a resonance testing machine with a maximum load of $F_{\max} = 600$ kN and a loading frequency of 60 Hz. The failure criterion

**Fig. 4** Scanning the surface of the weld toe with a laser sensor

of the fatigue test was defined as a frequency change of $\Delta f = \pm 0.15$ Hz.

To analyse the effect of an automated performed HFMI treatment on the geometry of the HFMI groove, the groove geometry was laser measured before the fatigue tests were carried out. Additionally, during some of the fatigue tests, infrared image sequences were recorded to investigate the crack initiation behaviour of robotic HFMI-treated welds in a subsequent evaluation.

4 Measurement of groove geometry

4.1 Procedure of the measurement

Before carrying out the fatigue tests, the groove geometry was surveyed by scanning the surface of the weld with a Keyence LJ-V7080 as shown in Fig. 4. The evaluation of the measurement data has been performed with an algorithm according to [8] using the software Matlab. The aim is to evaluate the effect of a robotic HFMI treatment on the indentation geometry and to validate the automated quality control integrated in the robot adaptation.

The raw data of the measurement is first obtained as a point cloud (see Fig. 5) with a resolution of 5 μm in the longitudinal direction of the weld and 50 μm in the transverse direction. Thus, the point cloud can also be interpreted as a sequence of cross sections of the weld, at intervals of 50 μm . Figure 6 shows the measurement of the groove-geometry parameters, depth, width and radius on a cross-section of the recorded weld profile.

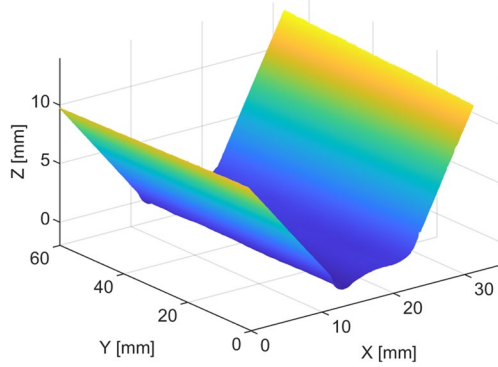


Fig. 5 3D profile of the scanned surface

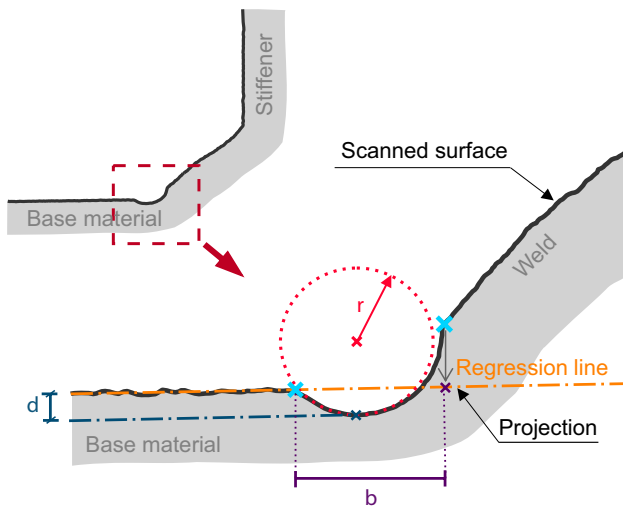


Fig. 6 Measurement of the groove geometry

In the first step, a spline function is fitted to the points of the measured cross section. The position of the groove within the weld toe can be determined, based on the edges of the indentation profile, which causes a local minimum in the course of the curvature of the fitted spline function. Afterwards, the geometry parameters can be calculated according to [8].

The indentation depth is in [8] defined by the point within the indentation profile which has the largest perpendicular distance to a regression line, fitted through the base material. Accordingly, the measurement of the indentation depth is performed by the calculation of the perpendicular distance of this point to the regression line. It could be recognised that the course of the regression line varies depending on the selected base material area. Thus, as Fig. 7 shows, using a regression line that includes the entire recorded base plate surface can lead to an underestimation of the measured indentation depth. Furthermore, measurements that include the entire base plate are not comparable to a conventional

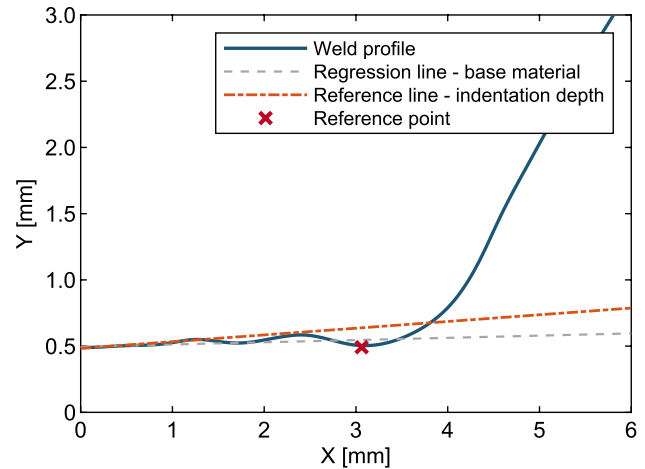


Fig. 7 Measurement of the groove depth using a reference line

control of the indentation depth, using manual gauges, as those methods only cover a short area of the base material. For this reason, the regression line was created over a base material area with a length of 2 cm. The described approach has already been validated by investigations in [11].

According to [8], the groove radius is determined by fitting a circle function to the indentation profile using the least square method. The radius of the rounded weld toe corresponds to the radius of the fitted circle function. As another parameter, the width is also determined according to the procedure described in [8]. At first, the projection points of the groove edges on the regression line are determined. The groove width is then measured as the distance between the projection points.

4.2 Results of the geometry measurement

As the manual HFMI treatment of series No. 3 was performed with a pin diameter of 4 mm, the results of the measurement are not comparable with the groove geometry of the automated treated welds, where the treatment was applied using a 3-mm pin. Therefore, in the following, only the geometry measurements of the samples, treated with a pin diameter of 3 mm, are presented. Figures 8 and 9 show the distribution of the measurements of the groove depth and the measured radius.

Regarding the mean values of the measured indentation depth, a difference between manual and automated treated weld toes can be noticed. Although the same pins were used for the manual and the robotic treatment, the robotic application of the HFMI treatment creates a deeper groove than the manually performed treatment. In this context, it must be considered that different treatment parameters were used for the robotic and the manual HFMI treatment (Table 3). Therefore, it is also possible

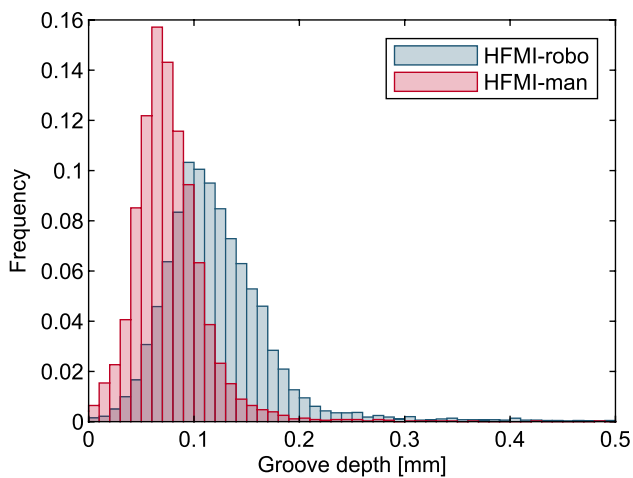


Fig. 8 Results of the measurement of the indentation depth

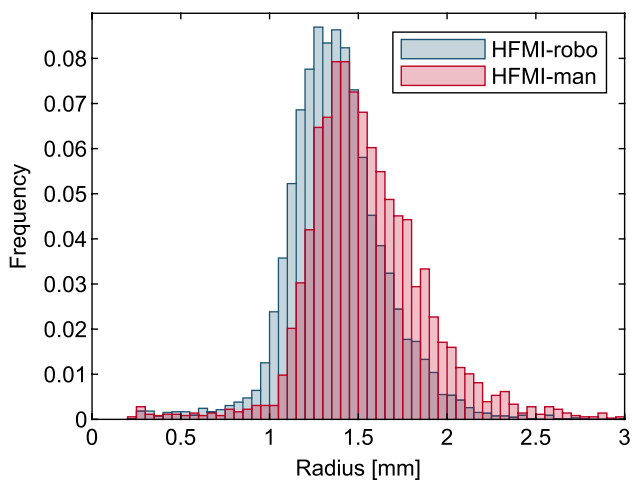


Fig. 9 Results of the measurement of the groove radius

that small differences in the measured indentation depth of manual and automated HFMI-treated weld toes are due to different treatment intensities. Additionally, as can be seen in Table 4, there is also a slight difference between the automated and manually performed treatment, concerning the variation of the depth measurements. Due to the lower variation of the automated created indentation

depth, the results indicate that by an adaptive robotic performed treatment, a more consistent groove geometry can be realised.

As expected, since the same pins were used for the HFMI treatment, regarding the measurements of the groove radii, there is no significant difference between the manual and the automated treated weld toes. Thus, both mean values fit the value of the pin radius used for the treatment quite well. Table 5 summarises the results of the measurement of the groove radii. Besides there is hardly any difference between the calculated variation of the measured radii, the evaluation of the groove radii indicates that, compared to a manual HFMI treatment, the effect of an adaptive robotic performed treatment on the treatment result is negligible. Therefore, the treatment result of an adaptive robotic HFMI treatment seems to be comparable to manual treatment.

In Fig. 10, the groove geometry is exemplary represented by polished sections of the different treatment conditions HFMI-man and HFMI-robo as well as a polished section of an AW specimen as a reference. For both HFMI-treated specimens, the plastic deformation of the weld toe compared to the AW condition is clearly visible. This matches the results of the measured pin radii which, as described before, also fit the value of the pin radius used for the treatment quite well. Regarding the indentations, created by the HFMI treatment, the low measured indentation depths are also illustrated by the polished sections. For the manually performed HFMI treatment (Fig. 10b) as well as the robotic HFMI treatment (Fig. 10c), hardly, any indentation depth can be noticed. Therefore, in the polished sections, no difference in the indentation depths of manual and automated HFMI-treated weld toes can be distinguished.

It can be noticed that the variation of the measured indentation depth as well as of the groove radii shows a slightly higher variation for manually performed treatment. Therefore, the results of the geometry measurements indicate that by an adaptive robotic HFMI treatment, compared to a manually performed treatment, a more consistent groove geometry can be realised. As there are no significant differences between the automated and manually performed treatment regarding the groove geometry, the HFMI groove created by an adaptive robotic HFMI treatment is considered to be comparable to the one, created by a manual treatment.

Table 4 Results of the measurement of the indentation depth

Series no	Weld condition	Pin diameter (mm)	Measurements (-)	Mean (mm)	Standard deviation (mm)	Variation coefficient (%)
No. 4	HFMI-man	3	3570	0.07	0.043	57%
No. 1	HFMI-robo (test application)	3	3449	0.12	0.060	52%
No. 2	HFMI-robo (praxis application)	3	3079	0.13	0.062	49%
No. 1 + 2	HFMI-robo	3	6546	0.12	0.062	51%

Table 5 Results of the measurement of the groove radius

Series no	Weld condition	Pin radius (mm)	Measurements (-)	Mean (mm)	Standard deviation (mm)	Variation coefficient (%)
No. 4	HFMI-man	1.5	3570	1.55	0.341	22%
No. 1	HFMI-robo (test application)	1.5	3449	1.43	0.266	19%
No. 2	HFMI-robo (praxis application)	1.5	3079	1.33	0.284	21%
No. 1 + 2	HFMI-robo	1.5	6546	1.38	0.279	20%

**Fig. 10** Polished sections of an AW specimen (a), a manual HFMI-treated weld toe (b) and an automated HFMI-treated weld toe (c)

5 Early crack detection by infrared thermography

To evaluate the crack initiation behaviour of automated and manually HFMI-treated welds, infrared thermography measurements were carried out during some of the fatigue tests. This method enables to investigate the cause of damage by analysing the temperature response of a specimen under an applied loading [17].

Using infrared thermography for early crack detection within a fatigue test is based on analysing the temperature response of a specimen under loading regarding the characteristic changes of the temperature response of the material, which is related to changing strain and material damage [17]. The temperature response of a sample under cyclic loading can be split into a linear part, which can be determined by the harmonic loading, and a nonlinear part, which describes the deviation of the temperature response from the linear temperature signal [18]. As fatigue-related processes like plasticisation as well as crack movement cause a significant local increase within the nonlinear temperature amplitude, analysing the nonlinearities allows the investigation of the damage behaviour of a sample [18]. Changes in linear temperature amplitude display stress redistributions; hence, crack initiation is additionally characterised by a significant local decrease in the linear temperature evolution, combined with an adjoining strong increase [17]. Therefore, analysing the temperature response of a sample depending on the number of

load cycles allows to investigate the damage behaviour. In [2], this approach has already been successfully applied to investigate the crack initiation and crack propagation behaviour of HFMI-treated welds.

5.1 Test procedure and preparation of specimens

In order to investigate the effect of a robotic performed HFMI treatment on the crack initiation behaviour, infrared thermography measurements were carried out simultaneously to several fatigue tests on automated and manual HFMI-treated specimens. Figure 11 shows the test setup of the fatigue tests with simultaneous infrared thermography measurements.

After regular intervals, image sequences were recorded by an infrared camera over a recording duration of 2 s with a recording frequency of 189 pictures per second. According to [18], the loading frequency of the fatigue tests was set to 7 Hz, so that around 27 pictures could be recorded per load cycle. An image sequence consists of 368 single images with a resolution of 320×253 pixels per image.

To ensure a direct comparability, the load levels of the fatigue tests, as well as the intervals after which the image sequences were recorded, were chosen to be the same for the automated and manually treated specimens. In Table 6, the test program of the fatigue tests with simultaneous infrared thermography measurements is displayed.

The areas, captured by the infrared camera, were covered with a graphite spray to ensure a consistent high emissivity

Fig. 11 Test setup of the fatigue tests with simultaneous infrared thermography measurements

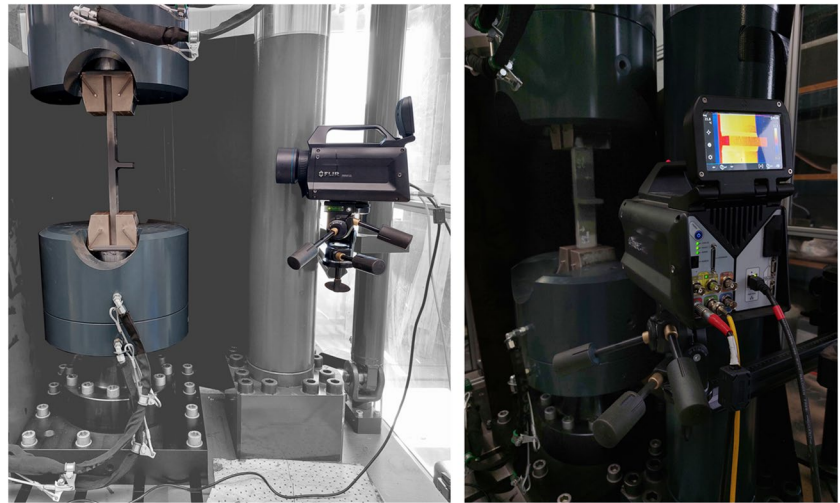


Table 6 Test program of the infrared thermography measurements

No	Series no	Weld condition	Pin Ø (mm)	$\Delta\sigma$ (N/mm ²)	N_f (-)	Intervals (number of load cycles)
1	No. 1	HFMI-robo	3	320	96,453	10,000
2	No. 1	HFMI-robo	3	360	23,030	500
3	No. 1	HFMI-robo	3	250	873,495	10,000
4	No. 2	HFMI-robo	3	320	157,362	10,000
5	No. 2	HFMI-robo	3	250	874,037	10,000
6	No. 3	HFMI-man	4	320	359,955	10,000
7	No. 3	HFMI-man	4	360	32,910	10,000
8	No. 4	HFMI-man	3	320	181,432	10,000
9	No. 4	HFMI-man	3	250	877,567	10,000

of the surface during the recording of the image sequences [18]. Within the evaluation of the infrared camera data, the relative displacement of the single images of an image sequence must be adjusted. Therefore, an aluminium reference marker is applied on the surface. Figure 12 shows an appropriately prepared specimen.

Evaluation of the infrared thermography data The raw data first consists of several image sequences, each including 368 pictures. The evaluation of these data sets is performed by an evaluation method that was developed by Medgenberg in [18]. As described in [17], the thermography data set must be prepared before the actual analysis of the recorded evolution of temperature. Therefore, at first, the intensity values recorded by the infrared camera are converted into temperature values. In a second step, the relative shift of the single images within a sequence is compensated with the help of the applied reference marker.

In the following analysis of the evolution of the temperature, the difference signal of every recorded pixel signal to a homogenous reference signal is determined. As a reference

signal, a pixel signal out of a less stressed field of the specimen is chosen, which, due to the harmonic evolution of the applied loading, adopts a nearly sinusoidal evolution as well.

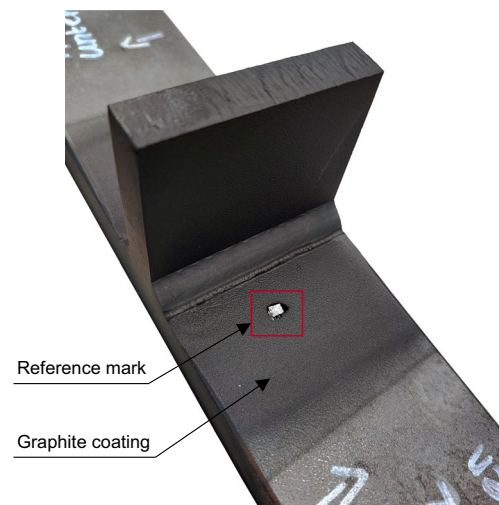


Fig. 12 Specimen prepared for infrared thermography measurements

For calculating the difference signal of a pixel signal, the determined reference signal is first fitted to the sequence of time of the pixel signal. For a further analysis of the temperature response, the linear and nonlinear temperature amplitudes are determined, based on the calculated difference signal to the applied load sequence. Afterwards, the damage behaviour can be investigated by a graphical evaluation of the linear and nonlinear temperature amplitudes.

5.2 Results of the infrared thermography measurements

5.2.1 Graphic evaluation of the temperature response

The graphic evaluation of the linear and nonlinear temperature distribution is explained below, using the example of a manually treated sample (specimen No. 9 in Table 6). Fig. 13 shows the linear and nonlinear temperature amplitudes in the centre of the specimen dependent on the numbers of load cycles.

The first picture represents the initial state after $N=40,000$ load cycles ($N/N_f=0.05$). Respecting that the distribution of the linear temperature amplitude indicates the stress field as well as stress concentrations, the weld toe is characterised by a significantly increased linear temperature amplitude compared to the nominal cross section as well as the area of the weld and the transverse stiffener, where the linear temperature amplitude is nearly homogeneous [17]. At the right side of the bottom weld toe, locally decreased linear temperature amplitudes can be recognised. Those punctually decreased linear temperature amplitudes within the weld toe shortly after the beginning of the fatigue test can be caused by defects near the surface such as weld spatter [18]. In the initial state, no or hardly, any nonlinearities can be found in the temperature response of the sample.

The infrared sequence recorded after $N=240,000$ load cycles ($N/N_f=0.27$) shows the point in time at which a significant increase in the nonlinearities first indicates local plasticisation. Changes in the linear temperature amplitude cannot be detected at this time.

Locally significantly reduced linear temperature amplitudes, combined with an increase in the direct adjacent areas, such as in the middle of the upper weld toe, indicate stress redistributions due to cracks [2]. After $N=420,000$ load cycles ($N/N_f=0.48$), in the same place as the increase of the non-linearities, a first very localised decrease of the linear temperature amplitude can be spotted; this can be taken as the point of crack initiation.

The infrared sequence after $N=700,000$ load cycles ($N/N_f=0.72$) exemplary displays the temperature response of the specimen at a later state of the fatigue test, after advanced crack propagation. Compared to an earlier state, an increase of the non-linearities in the area of the damage leading to failure can be noticed. The linear temperature amplitude has further decreased, combined with an increase in the directly adjacent areas, which indicates stress redistributions caused by the crack.

The last picture belongs to the last image sequence, recorded after $N=870,000$ load cycles ($N/N_f=0.99$) just before the end of the fatigue test. Strongly increased linear temperature amplitudes in the remaining cross-section at the edges of the sample indicate the stress concentrations, due to the crack in the middle of the upper weld toe. The non-linearities around the crack have become zero as the crack growth has progressed so far that there is no more temperature transfer. Only small areas with increased non-linear temperature amplitudes at the edge of the crack indicate the plasticising of the crack tips.

As another example, Fig. 14 shows the distribution of the linear and nonlinear temperature amplitudes of an automated treated sample (specimen No. 3 in Table 6) dependent on the number of load cycles. The graphic evaluation of the temperature evolution corresponds to the results for the manually treated specimen presented in Fig. 13. In the following, the evaluation of the crack initiation and propagation behaviour is presented using the data of the two samples shown in Figs. 13 and 14.

Evaluation of the crack propagation behaviour According to [2], the crack propagation can also be displayed using contour lines, representing a defined magnitude of deviation of the temperature $\Delta\vartheta$ of the linear and nonlinear temperature amplitudes compared to the initial state in dependence on the number of load cycles. Figure 14 shows the crack propagation of a manually treated sample (sample No. 9 in Table 6). Figure 15 exemplary presents an automated treated sample (No. 3 in Table 6). Since there were no beach mark tests carried out and the point of crack initiation can therefore not be determined exactly, only a qualitative comparison of the temperature response of the manual and automated HFMI-treated samples has been carried out. Due to the lack of the possibility of matching with beach marks, the magnitude of the deviation of the temperature amplitudes $\Delta\vartheta_{lin}$ and $\Delta\vartheta_{nlin}$ used in the evaluation was chosen according to [2]. The aim is a qualitative comparison of the crack propagation behaviour of the automated and manual HFMI-treated samples.

Fig. 13 Distribution of the linear and nonlinear temperature amplitudes in the centre of the manually treated specimen tested with $\Delta\sigma = 250 \text{ N/mm}^2$, after a specific number of load cycles; left, linear temperature amplitudes; right, nonlinear temperature amplitudes

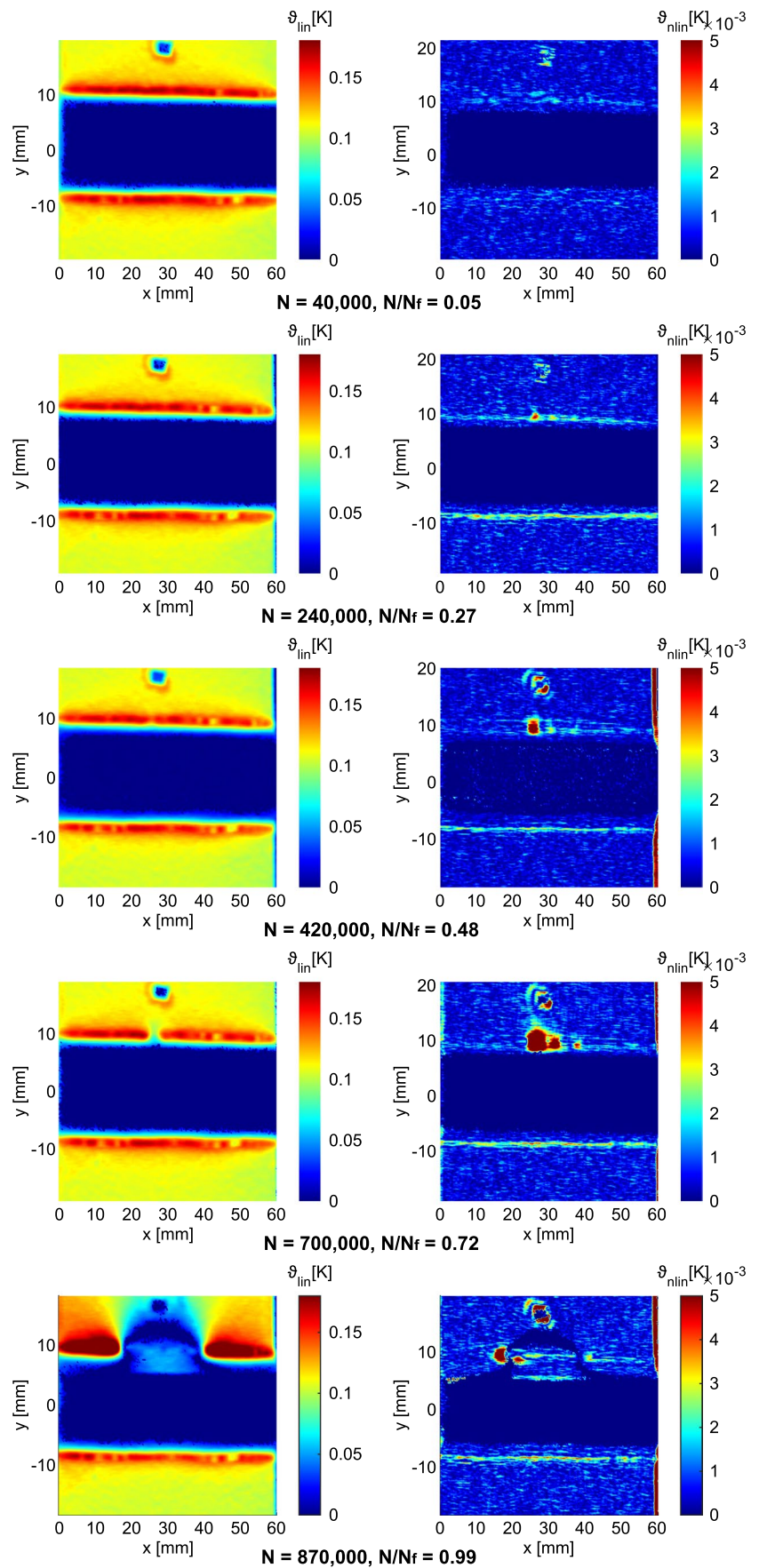
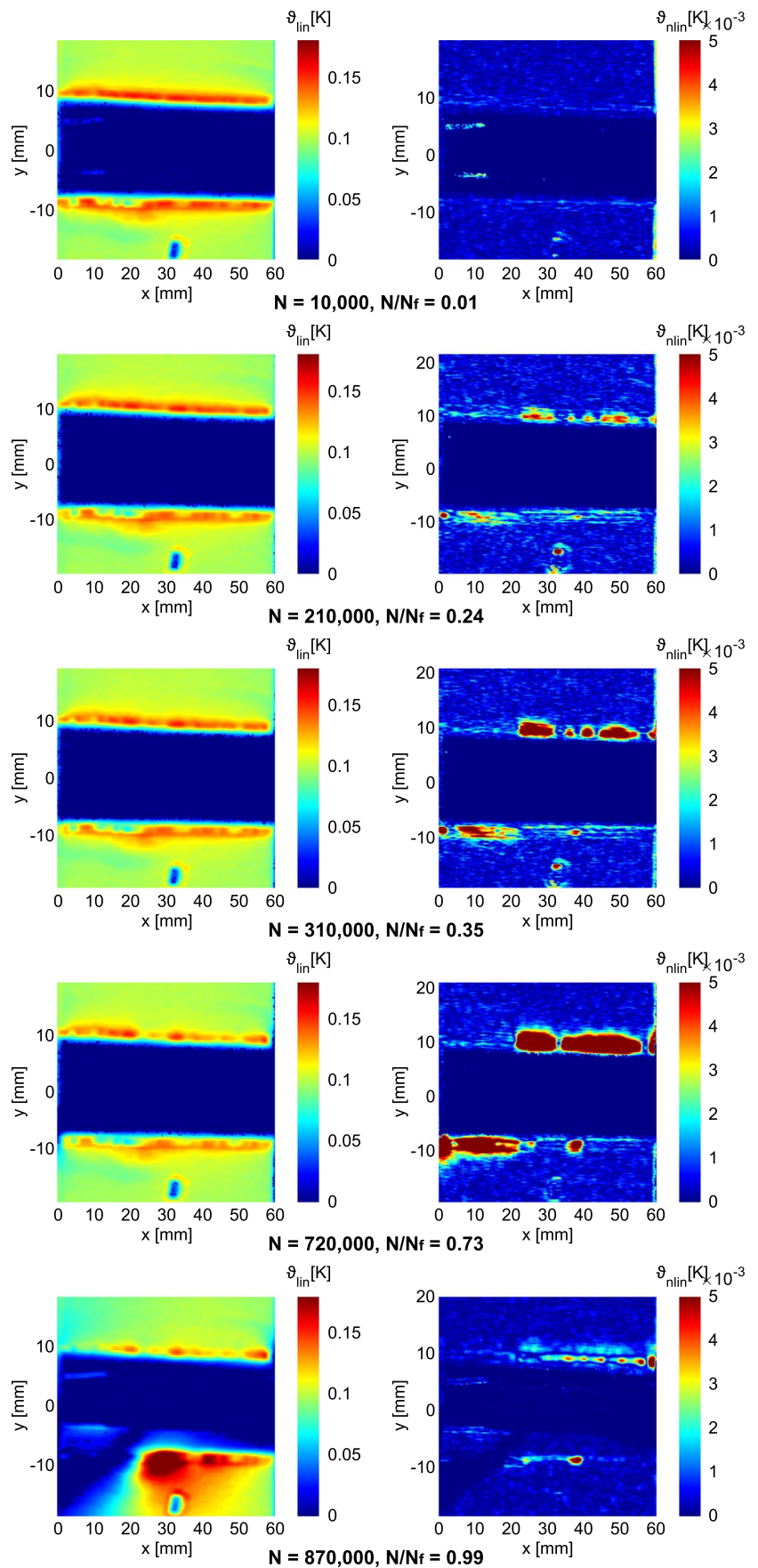


Fig. 14 Distribution of the linear and nonlinear temperature amplitudes in the centre of the automated treated specimen tested with $\Delta\sigma = 250 \text{ N/mm}^2$, after a specific number of load cycles; left, linear temperature amplitudes; right, nonlinear temperature amplitudes



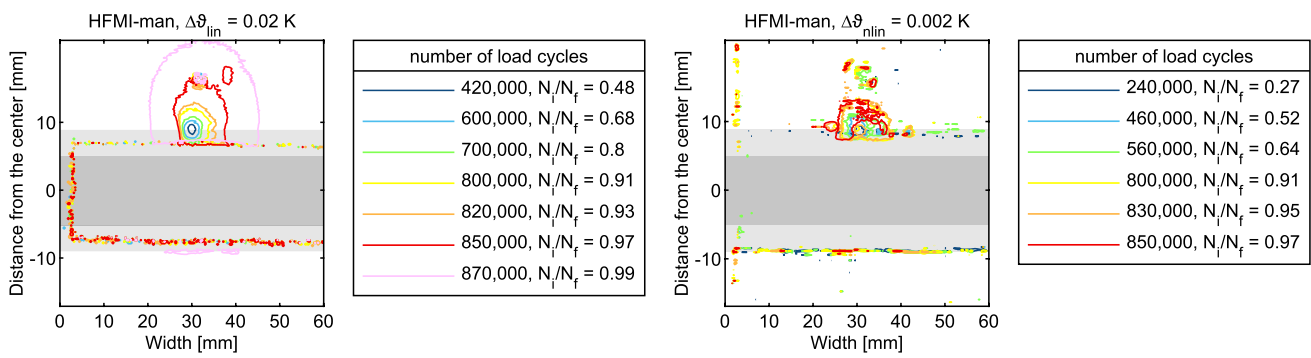


Fig. 15 Crack propagation of a manually treated sample tested with $\Delta\sigma=250 \text{ N/mm}^2$, represented by a difference amount $\Delta\theta$ of the linear and nonlinear temperature amplitudes compared to the initial state

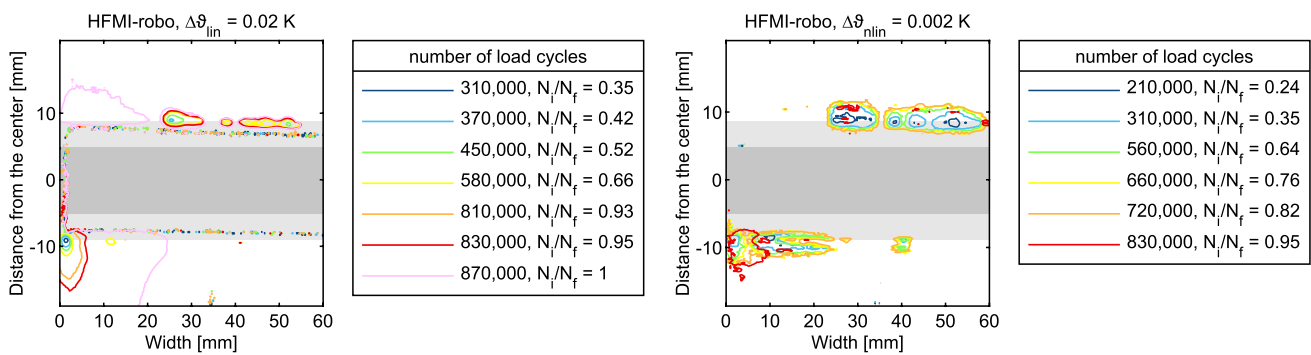


Fig. 16 Crack propagation of an automated treated sample tested with $\Delta\sigma=250 \text{ N/mm}^2$, represented by a difference amount $\Delta\theta$ of the linear and nonlinear temperature amplitudes compared to the initial state

When comparing the contour lines, it can be noticed that only a single crack appears during the entire course of damage of the manually treated sample (Fig. 15), while the damage progression of the automated HFMI-treated specimen (Fig. 16) is characterised by the occurrence of several incipient cracks. As this could not be confirmed by the evaluation of the other samples, the number of cracks occurring is not seen as a characteristic difference between manual and automated treatment. The focus of further evaluation therefore lays on differences of the crack initiation phase. For a qualitative comparison, the image sequence, for which a deviation magnitude of $\Delta\theta \sim 0.02 \text{ K}$ within the linear temperature amplitude could first be recognised, was defined as technical crack initiation. In Fig. 17, the results of the qualitative evaluation of the crack initiation are presented as the ratio of the number of crack load cycles to the number of fracture load cycles at the respective stress range.

Since the points of the determined ratio of the number of crack load cycles to the number of fracture load cycles are close to each other at all the tested load levels, no significant difference between a manually performed and an automated HFMI treatment could be noticed in the

evaluation. Therefore, the crack initiation behaviour of automated HFMI-treated weld toes seems to be comparable to manually treated weld toes.

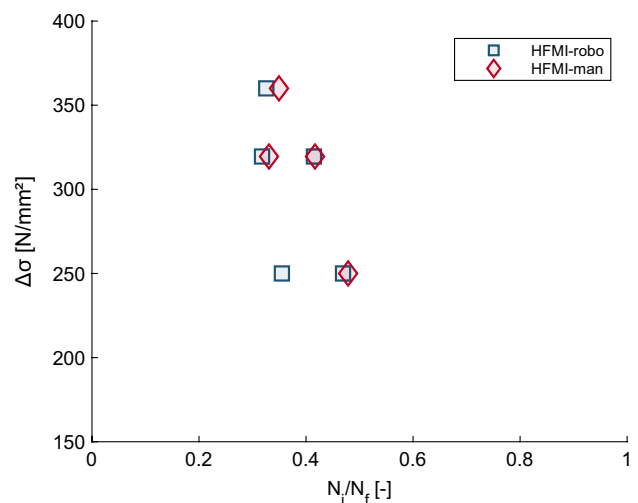


Fig. 17 Qualitative evaluation of the crack initiation

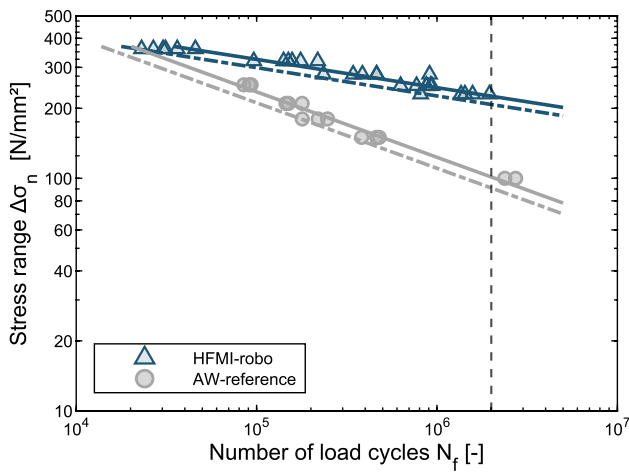


Fig. 18 S–N curve of the automated treated specimen

6 Test results

Figures 17 and 18 present the S–N curves for the automated and manually treated samples, calculated according to [19]. Corresponding to this approach, the mean fatigue resistance $\Delta\sigma_{50\%}$ for a survival probability $P = 50\%$ was computed based on a linear regression. The characteristic S–N curves were determined, using a one-sided lower 95% prediction bound, and therefore represent a survival probability of $P = 95\%$. The calculated reference value of the fatigue strength $\Delta\sigma_c$ as well as the mean value $\Delta\sigma_{50\%}$ is given for $N_c = 2 \times 10^6$ load cycles, as shown in Table 7.

As there is no difference in the treatment parameters of the two series with automated HFMI-treated specimen, they are summarised in the statistical evaluation shown in Fig. 18. The manual HFMI treatment was applied using two different pin radii. Thus, the two HFMI-man series were first evaluated separately. The results of the separate evaluation can be taken from Table 7. Outliers, such as samples with failure in the load application as well as run outs with more than $N = 5 \times 10^6$ load cycles, were not considered in the statistical evaluation. Regarding the calculated values of the fatigue

strength, as well as the slope of both HFMI-man series, no significant difference can be found. This indicates that the influence of the pin diameter on the HFMI treatment result is negligible for these series. Therefore, the test results of the manually treated specimens were summarised in one S–N curve, shown in Fig. 19.

For a comparison of the test results of manual and automated performed HFMI treatment, both S–N curves are displayed in Fig. 20. The statistical investigation of the results of the AW reference by a linear regression resulted in a slope of $m = 3.55$ and a characteristic fatigue strength of $\Delta\sigma_c = 90 \text{ N/mm}^2$. Thus, the results of the AW reference series confirmed to the fatigue class (FAT) 80, according to [20], quite well.

According to the IIW recommendations [21] and the DAST guideline [22], the considered notch detail of a transverse stiffener made of S355 with HFMI-treated weld toes is assigned FAT 140. With the calculated characteristic values of the fatigue strength of $\Delta\sigma_{c, \text{HFMI-man}} = 202 \text{ N/mm}^2$ and $\Delta\sigma_{c, \text{HFMI-robo}} = 207 \text{ N/mm}^2$, both manual and automated HFMI treatment show a higher characteristic fatigue strength, compared to the specified FAT 140.

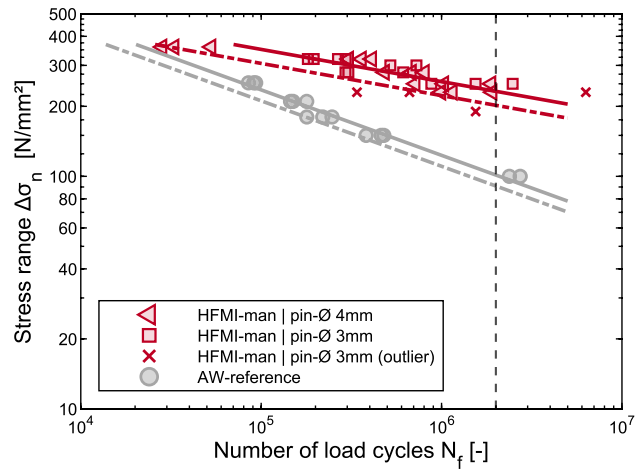


Fig. 19 S–N curve of the manually treated specimen

Table 7 Results of the fatigue tests

Series no	Number of specimens	Weld condition	Slope	Standard deviation	Scatter, T_N	Fatigue strength	
						$\Delta\sigma_{50\%}$ (N/mm ²)	$\Delta\sigma_c$ (N/mm ²)
No. 1	15	HFMI-robo	8.21	0.17	1:2.76	223	203
No. 2	14	HFMI-robo	8.29	0.17	1:2.52	228	209
No. 1+2	29	HFMI-robo	8.22	0.16	1:2.62	225	207
No. 3	15	HFMI-man	7.37	0.26	1:4.81	229	195
No. 4	15	HFMI-man	6.88	0.21	1:3.41	234	201
No. 3+4	30	HFMI-man	7.22	0.24	1:4.13	232	202
No. 5	14	AW	3.55	0.08	1:1.62	101	90

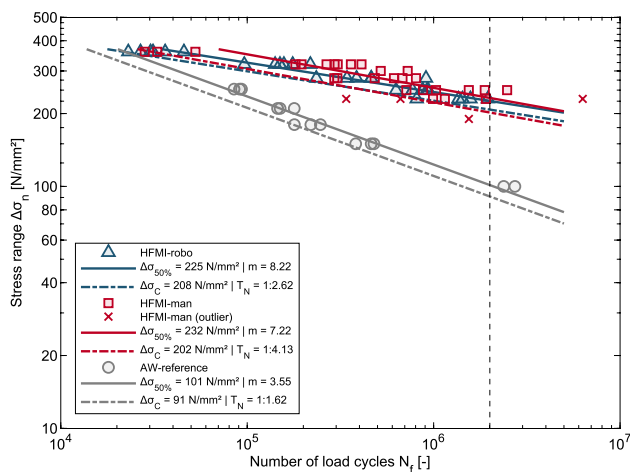


Fig. 20 S–N curves of the automated and manually treated specimen

A comparison of the S–N curves of both treatment states HFMI-man and HFMI-robo in Fig. 20 shows that there is no considerable difference in the fatigue results of the automated and manually treated specimens. Regarding the different treatment parameters used for the automated and the manually performed treatment, this is in agreement with results of previous studies like [3, 15, 16] where no significant effect of varying treatment intensities on the fatigue strength was observed either. As there is no significant difference between the calculated characteristic values of the fatigue strength with $\Delta\sigma_{c, \text{HFMI-man}} = 202 \text{ N/mm}^2$ and $\Delta\sigma_{c, \text{HFMI-robo}} = 207 \text{ N/mm}^2$, the results indicate that an automated performed adaptive application of the HFMI treatment, which is able to adapt to irregularities in the course of the weld toe, enables the same increase of the fatigue strength as a common manual HFMI-treatment. In contrast, the statistical evaluation shows a difference in the scatter of the test results. With $T_{N, \text{HFMI-robo}} = 1:2.62$ and $T_{N, \text{HFMI-man}} = 1:4.13$, the lower scatter of the fatigue test results of the automated HFMI-treated samples implies that a more consistent treatment quality can be reached, using an adaptive automated HFMI treatment. Based on the test results, it is assumed that an automated HFMI treatment, performed using an adaptive robotised HFMI application, achieves a treatment quality, which is at least comparable to the results achieved by a manual applied treatment.

7 Conclusion

The aim of this work was to evaluate the effect of an adaptive robotic HFMI treatment on the groove geometry, the crack initiation behaviour and the achieved increase of the fatigue strength compared to a common, manually performed HFMI treatment. For this purpose, several experimental investigations were carried out on the notch detail transverse stiffener.

Measurements of the groove geometry revealed that the differences between automated and manually performed HFMI treatment, regarding the consistency of the geometry parameters as well as the evaluated mean values, are negligible. Additionally, the smaller variation of the groove geometry indicates that the HFMI groove, created by the developed adaptive robotic HFMI treatment, offers the potential to realise a more consistent groove geometry.

In order to evaluate the crack initiation behaviour of automated and manual HFMI-treated welds, infrared thermography measurements were carried out, simultaneous to some of the fatigue tests. The qualitative evolution of damage was evaluated, based on the recorded infrared sequences. Similar to the results of the geometry measurements, no significant difference between robotic and manual HFMI treatment could be detected in a qualitative comparison of the crack propagation. For a more precise evaluation of the crack initiation as well as the continuing crack propagation, in further research, infrared thermography measurements should be accompanied by fatigue tests, creating beach marks, as performed in [2].

Based on the results of the fatigue tests, the effectiveness of an adaptive robotic HFMI treatment regarding the achieved increase of the fatigue strength could be confirmed. As the statistical evaluation of the test results showed, the calculated fatigue strength, achieved by the adaptive robotic and the manual treatment, was almost the same. Thereby, the lower scatter of the test results of the automated treated specimens indicates that an adaptive automated HFMI treatment can result in a more consistent treatment result, compared to a manually performed treatment.

The results of the experimental work therefore confirmed the effectiveness of an adaptive robotic HFMI treatment, using the developed HiFIT application. It is assumed that the treatment quality, achieved by the automated application, is at least comparable to the treatment, resulting from a manually performed treatment, while the robotic application has the potential to minimise the scatter of the treatment result and, thus, realise a more consistent treatment quality.

In order to enable a greater more diverse use of the robotic HFMI treatment, future investigations should focus on further details. In this context, the practicability and the achieved treatment result of automated treatment on more complex component geometries are of interest.

Supplementary Information The online version contains supplementary material available at <https://doi.org/10.1007/s40194-024-01701-z>.

Funding Open Access funding enabled and organized by Projekt DEAL. The research project “Use of robot technology for the automation of higher-frequency hammering processes” (RobAH) of the Central Innovation Programme for SMEs (ZIM) was funded by the Federal Ministry of Economics and Climate Protection (BMWK) based on a resolution of the German Bundestag.

Declarations

Conflict of interest The authors declare no competing interests.

Open Access This article is licensed under a Creative Commons Attribution 4.0 International License, which permits use, sharing, adaptation, distribution and reproduction in any medium or format, as long as you give appropriate credit to the original author(s) and the source, provide a link to the Creative Commons licence, and indicate if changes were made. The images or other third party material in this article are included in the article's Creative Commons licence, unless indicated otherwise in a credit line to the material. If material is not included in the article's Creative Commons licence and your intended use is not permitted by statutory regulation or exceeds the permitted use, you will need to obtain permission directly from the copyright holder. To view a copy of this licence, visit <http://creativecommons.org/licenses/by/4.0/>.

References

- Ummerhofer T, Telljohann G, Dannemeyer S et al (2010) Abschlussbericht des Forschungsprogramms REFRESH Lebensdauererlängerung bestehender und neuer geschweißter Stahlkonstruktionen [Report of the research project REFRESH extension of the service life of existing and new welded steel constructions]. Versuchsanstalt für Stahl, Holz und Steine, Karlsruher Institut für Technologie (KIT), Karlsruhe (in German)
- Weich I (2008) Ermüdungsverhalten mechanisch nachbehandelter Schweißverbindungen in Abhängigkeit des Randschichtzustands [Fatigue behaviour of mechanical post weld treated welds depending on the edge layer condition]. Technischen Universität Carolo-Wilhelmina zu Braunschweig (in German). <https://doi.org/10.24355/dbbs.084-200903300200-1>
- Kuhlmann U, Ummerhofer T, Breunig S, Weidner P (2018) 1/2018 Forschungsbericht - Entwicklung einer DASt-Richtlinie für Höherfrequente Hämmerverfahren [P (2018) 1/2018 Research report - Development of a DASt guideline for high frequency hammer peening]. Deutscher Ausschuss für Stahlbau e.V. (in German). https://dast.deutscherstahlbau.de/fileadmin/user_upload/DASt/DASt-Forschungsberichte/2018-1_AiF17886_Schlussbericht.pdf
- Berg J (2016) Einfluss des Höherfrequenten Hämmerens auf die Ermüdungsfestigkeit geschweißter ultrahochfester Feinkornbaustähle [Influence of high frequency hammer peening on the fatigue strength of welded ultra high strength fine grained structural steels]. Universität Duisburg-Essen (in German). <https://doi.org/10.2370/9783844049787>
- Weich I, Ummerhofer T, Nitschke-Pagel T et al (2009) Fatigue behaviour of welded high-strength steels after high frequency mechanical post-weld treatments. *Weld World* 53:R322–R332. <https://doi.org/10.1007/BF03263475>
- Ummerhofer T, Weich I (2006) REFRESH – Lebensdauererlängerung bestehender und neuer geschweißter Stahlkonstruktionen [REFRESH - Extension of the fatigue life of existing and new welded steel structures]. *Stahlbau* 75:605–607. <https://doi.org/10.1002/stab.200690079>(inGerman)
- Yildirim HC, Marquis GB (2012) Overview of fatigue data for high frequency mechanical impact treated welded joints. *Weld World* 56:82–96. <https://doi.org/10.1007/BF03321368>
- Mikkelsen AF, Kristiansen M, Kristiansen E (2022) Development of an automated system for adaptive post-weld treatment and quality inspection of linear welds. *Int J Adv Manuf Technol* 119:3675–3693. <https://doi.org/10.1007/s00170-021-08344-0>
- Tehrani Yekta R, Ghahremani K, Walbridge S (2013) Effect of quality control parameter variations on the fatigue performance of ultrasonic impact treated welds. *Int J Fatigue* 55:245–256. <https://doi.org/10.1016/j.ijfatigue.2013.06.023>
- Ghahremani K, Safa M, Yeung J et al (2015) Quality assurance for high-frequency mechanical impact (HFMI) treatment of welds using handheld 3D laser scanning technology. *Weld World* 59:391–400. <https://doi.org/10.1007/s40194-014-0210-3>
- Wendler L, Löschner D, Engelhardt I et al (2023) Automatisierte Schweißnahtnachbehandlung durch höherfrequentes Hämmeren. *Stahlbau* 92(7):418–426. <https://doi.org/10.1002/stab.202300021>
- EN 10149–1:2013–12: Hot rolled flat products made of high yield strength steels for cold forming Part 1: General technical delivery conditions; German version
- EN ISO 14341:2020–12: Welding consumables - wire electrodes and weld deposits for gas shielded metal arc welding of non alloy and fine grain steels - Classification (ISO 14341:2020); German version
- EN ISO 14175:2008–06: Welding consumables - gases and gas mixtures for fusion welding and allied processes (ISO 14175:2008); German version
- Kuhlmann U, Breunig S, Gözl L-M (2019) Untersuchungen zur Auswirkung variierender Ausführungsqualitäten einer HFH-Nachbehandlung und Beurteilung einfacher Methoden zur Überprüfung der Nachbehandlungsspur [Investigations on the effect of varying execution qualities of an HFMI-treatment and assessment of simple methods for verifying the treatment groove]. Universität Stuttgart, Institut für Konstruktion und Entwurf (in German). https://www.baw.de/content/publikationen/www-dokumente-oeffentlich/0/2019_01_30_Schlussbericht_Final.pdf
- Schubnell J, Hanji T, Tateishi K, et al (2022) Quantifying the intensity of high frequency mechanical impact treatment. IIW-document XIII-2930–22. In: 75th International Institute of Welding Annual Assembly. Tokyo, Japan
- Medgenberg J, Ummerhofer T (2007) Ortsaufgelöste Detektion von Ermüdungsvorgängen in metallischen Werkstoffen mit Infrarot-Thermografie [Locally resolved detection of fatigue processes in metallic materials with infrared thermography]. TU Braunschweig, Institut für Bauwerkserhaltung und Tragwerk, Braunschweig (in German)
- Medgenberg J (2007) Investigation of localized fatigue properties in unalloyed steels by infrared thermography. Technischen Universität Carolo-Wilhelmina zu Braunschweig. <https://doi.org/10.24355/dbbs.084-200803070100-6>
- Drebenstedt K, Euler M (2018) Statistical analysis of fatigue test data according to eurocode 3. In: Maintenance, safety, risk, management and life-cycle performance of bridges: proceedings of the Ninth International Conference on Bridge Maintenance, Safety and Management (IABMAS 2018), Melbourne, Australia, 9–13 July 2018. CRC Press, London, pp 2244–2251
- Hobbacher AF (2016) Recommendations for fatigue design of welded joints and components; IIW document IIW-2259–15 ex XIII-2460–13/XV-1440–13, 2nd ed. 2016. Springer International Publishing : Imprint: Springer, Cham. <https://doi.org/10.1007/978-3-319-23757-2>
- Marquis GB, Zuheir B IIW Recommendations on high frequency mechanical impact (HFMI) treatment for improving the fatigue strength of welded joints; IIW-document XIII-WG2–147–15
- Deutscher Ausschuss für Stahlbau DASt (2019) DASt - Richtlinie 026 - Ermüdungsbemessung bei Anwendung höherfrequenter Hämmerverfahren [DASt (2019) DASt - Guideline 026 - Fatigue design for the application of high frequency hammer peening methods]. Stahlbau Verlags- und Service GmbH, Düsseldorf (in German)

Publisher's Note Springer Nature remains neutral with regard to jurisdictional claims in published maps and institutional affiliations.